POLITECNICO DI TORINO
Repository ISTITUZIONALE

Measurement and Computation of Nb3Sn Rutherford Cables Strength Under Multi-Axial Loading Conditions

Original
Measurement and Computation of Nb3Sn Rutherford Cables Strength Under Multi-Axial Loading Conditions / Vallone, G., Croteau, J., Anderssen, E., Bordini, B., D'Addazio, M., Ferracin, P., Niccoli, F.. - In: IEEE TRANSACTIONS ON APPLIED SUPERCONDUCTIVITY. - ISSN 1051-8223. - 34:5(2024), pp. 1-5. [10.1109/TASC.2023.3340126]

Availability:
This version is available at: 11583/3003519 since: 2026-04-08T08:49:01Z

Publisher:
Institute of Electrical and Electronics Engineers Inc.

Published
DOI:10.1109/TASC.2023.3340126

Terms of use:

This article is made available under terms and conditions as specified in the corresponding bibliographic description in the repository

Publisher copyright
IEEE postprint/Author's Accepted Manuscript

©2024 IEEE. Personal use of this material is permitted. Permission from IEEE must be obtained for all other uses, in any current or future media, including reprinting/republishing this material for advertising or promotional purposes, creating new collecting works, for resale or lists, or reuse of any copyrighted component of this work in other works.

(Article begins on next page)

02 November 2026

This article has been accepted for publication in IEEE Transactions on Applied Superconductivity. This is the author's version which has not been fully edited and content may change prior to final publication. Citation information: DOI 10.1109/TASC.2023.3340126

Measurement and Computation of Nb_3Sn Rutherford Cables Strength Under Multi-Axial Loading Conditions

G. Vallone, J.F. Croteau, E. Anderssen, B. Bordini, M. D'Addazio, P. Ferracin, F. Niccoli

***Abstract*—Superconducting magnet coils are subject to large thermo-mechanical loads applied during magnet assembly, cooldown and operation. These loads can cause the reduction of their critical current due to mechanical strains or local filament failures. Measurements on longitudinally stretched strands and Rutherford cables under transverse pressure have allowed exploration of material limits in two directions. However, no systematic study of the effect of multi-axial loading conditions has been done. Finite Element (FE) models show that, indeed, the actual limits of the material are strongly dependent on the nature of the applied load and that the strength under multi-axial loading can be significantly higher with respect to uniaxial loading conditions. In this paper, we try, for the first time, to measure the effect of multi-direction loading conditions on Nb_3Sn Rutherford cables. The experiments are performed on impregnated cable stacks under transverse, lateral, and longitudinal constraints. The integrity of the cables is verified by destructive metallography inspection, evaluating the damage as a function of the applied loading condition.**

***Index Terms*—Nb_3Sn , Mechanical Strength, Rutherford Cable**

I. Introduction

PREDICTING the mechanical limits of Nb_3Sn coils is a crucial and yet difficult task, fundamental for the correct design of superconducting magnets. An univocal definition of strength cannot be established: for example, one could assume as limit any stress that could lead to a reduction in magnet performances. This does not have to coincide with actual failures inside the coil composite, as the critical current of Nb_3Sn is a function of the applied strain [1]. On the other hand, the composite can fail in many ways, and some of these (e.g. bonding failure) do not always result in decreased performances of the magnet. In previous works, the same authors showed how the reversible effects can be introduced in magnet designs using the exponential strain function and multi-scale modeling approaches [1]–[3]. In this study, instead, the strength limit is considered as the onset of the irreversible effects. Potentially, the strain function could be used also in this region, as already proposed in [4], but the approach lacks experimental proof for the moment.

Magnet designers commonly use two different failure criteria: a non-interacting one, with a limit on the transverse or azimuthal stress of 150/175 MPa, and an interacting criterion that limits the Von Mises equivalent stress below 150/200 MPa [5]. The former criterion is based on the critical current reduction measured on transversally loaded cables [6], while the latter has been established with consistent comparison between finite element (FE) models and magnet test results [7]. Both these criteria should not be generally applicable to composites (such as Nb_3Sn coils), since these materials usually show significant anisotropy in the failure surface, and different failure modes caused by different load combinations [8]–[10].

Many different failure modes were identified in the past. Experiments on stacks of impregnated cables showed shear failure under azimuthal loading, and delamination/debonding failures under radial loads [11]. Some authors tried to measure the shear failure limits using short beam shear experiments [12]; and many designs try to avoid debonding failures at the coil/winding pole interfaces. Some attempts were also made to introduce the debonding failures of these interfaces in numerical models [13], [14]. Micrography imaging of superconducting strands and cables after transverse loading allowed to identify cracks propagating inside the filaments both radially and along their length [6], [15]. It is not clear if there is a connection between radial and longitudinal cracks: for example, if the cracks form as radial and then propagate along the length. Measurements have shown that, until the filament continuity is completely interrupted, the cracks do not correspond to a reduction of the current carrying capability of the conductor. As a consequence, radial cracks are not dangerous per-se, but only if they can propagate in the longitudinal direction, cutting the filament. Finally, metallurgical investigations on tested superconducting coils allowed to identify failures at the insulation level, and net cross-section ('chopped') failure of filaments [16].

This paper investigates the strength of Nb_3Sn coils : first using a multi-scale numerical model to define non-interactive and interactive orthotropic failure limits; and then with measurements performed on impregnated MQXF cable stacks under uni-axial and bi-axial loading conditions. The relevant strand and cable parameters can be found in [17].

Automatically generated dates of receipt and acceptance will be placed here

This work was supported by the U.S. Department of Energy, Office of Science, Office of High Energy Physics, through the Magnet Developemtn Program.

G. Vallone, J.F. Croteau, E. Anderssen, M. D'Addazio and P. Ferracin are with Lawrence Berkeley National Laboratory, Berkeley, CA 94720 USA (e-mail: gvallone@lbl.gov).

B. Bordini is with the European Organization for Nuclear Research (CERN), 1211 Geneva, Switzerland

M. D'Addazio is with Politecnico di Torino, 10129 Torino (TO), Italy

F. Niccoli is with Università della Calabria, 87036 Rende (CS), Italy

Colour versions of one or more of the figures in this paper are available online at http://ieeexplore.ieee.org.

Digital Object Identifier: xx

© 2023 IEEE. Personal use is permitted, but republication/redistribution requires IEEE permission. See https://www.ieee.org/publications/rights/index.html for more information.

This article has been accepted for publication in IEEE Transactions on Applied Superconductivity. This is the author's version which has not been fully edited and content may change prior to final publication. Citation information: DOI 10.1109/TASC.2023.3340126

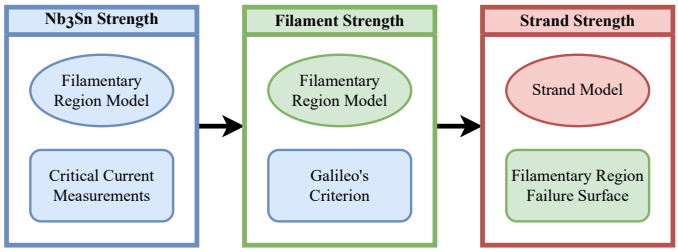


Fig. 1. Flowchart for strength computation of the coil composite with multi-scale modeling. The strength limits computed on subscale RVE models are transferred to higher scale models.

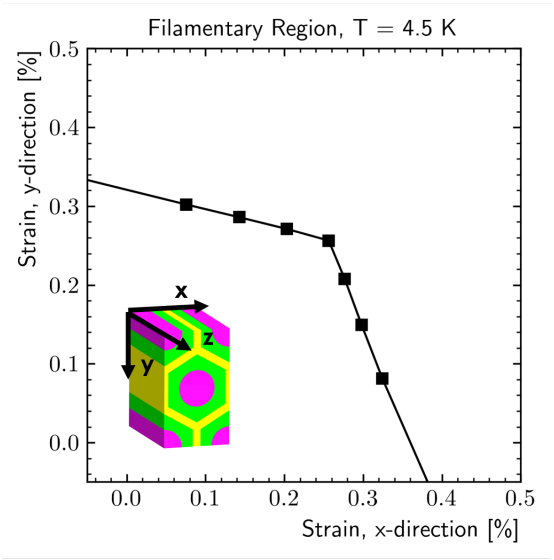


Fig. 2. Failure surface of the filamentary region under bi-axial strain states applied in the x-y plane. The model components are, starting from the center, a partially filled bronze core, a Nb_3Sn region, and a copper matrix.

II. Multi-Scale Strength Modeling

A multiscale 3D Representative Volume Element (RVE) approach is used to model the coil composite, following the methodology proposed in [2], [5]. Three FE models are built: one for the filamentary region, one for the strand, and one for the cable stack. The material properties for the constituents were extracted from literature. Reference values can be found in [2]. To correctly match the resulting anisotropic plastic behaviour introduced by copper yielding, the model requires an anisotropic yield strength criterion and an anisotropic work hardening rule. Here we use the Hill yield surface and a generalized Hill hardening model.

To compute the overall composite strength, a multi-scale approach is used: at each stage, the lower-scale model is used to obtain limits for the region homogenized at the higher-scale level model. An overview of the entire process is provided in Fig. 1: stresses computed with the filamentary region are compared to experiments to estimate the strength of Nb_3Sn ; then, the same model is tested under multi-axial loads to define a failure surface for the filamentary region of the strand model. Failure is assumed when the maximum principal stress exceeds the Nb_3Sn strength. Finally, the strand model is tested under multi-axial loads and the failure surface is found checking the stresses against the previously defined surface. The process is repeated again at the coil level (not shown in Fig. 1).

A. Filament Strength

Since Nb_3Sn is a fragile material, its strength is dictated by its fracture toughness, and the size of the defect that determines the failure. Unfortunately, no clear measurements of the fracture toughness at cold are available, and the typical defect size is unknown. On the other hand, measurements on uniaxially loaded strands show irreversible degradation starting from an intrinsic strain of 0.38% (at 4 K) [18]. It is possible to compare this result with the stress computed applying a uniform axial strain to the filamentary region model shown in Fig. 2. In this load case, the Nb_3Sn volume experiences a relatively uniform maximum principal stress of 400 MPa. Assuming that the measured critical current degradation is due to the sudden propagation of the inner defects, we can deduce that this is the stress at which a typical defect propagates into a crack at 4.5 K, and use this information to compute the filament strength under different loading conditions. The failure is assumed to occur on the surface surrounding the filament core. This is because this surface, after reaction, is expected to contain the largest defects, as confirmed by previous experiments showing that the cracks are originating almost exclusively from this area [6].

The resulting failure surface, as a function of the applied strain in the filament cross-section, is shown in Fig. 2. The failure limit in the filament plane is slightly different than along the length, and equal to a strain of 0.36% in the x-direction, and 0.32% in the y-direction. Applying bi-axial tensile stress states results in a reduction of the failure limit up to a value of 0.25% on the $(\varepsilon_x = \varepsilon_y, \sigma_z = 0)$ line.

B. Coil Strength

The limits computed on the filament model can be scaled to the strand model assuming that the filamentary region will experience crack propagation when the strains exceed the values computed at the previous step. Similarly, the process can be extended to compute the strength up to the coil level. In reality, the difference between strand strength and coil strength is almost negligible with this approach. The flowchart in Fig. 1 illustrates the process followed up to the strand level.

Neglecting the effect of multi-axial stress states, one can compute uni-axial stress limits for the coil composite under tension, compression and shear loads:

$$\begin{Bmatrix} S_x^- \\ S_y^- \\ S_z^-/S_z^+ \end{Bmatrix} = \begin{Bmatrix} 155 \\ 115 \\ 167/162 \end{Bmatrix} \text{MPa} \qquad (1)$$

where S is the strength, x, y, z are the load directions (see Fig. 3), and $-, +$ the load sign, compressive and tensile respectively. The difference between S_x and S_y is due to the filament and strand asymmetry. The computed in-plane tensile limits of the coil are unrealistically high (118 and 78 MPa in the x and y direction respectively), as the composite is expected to experience debonding failures at lower stresses. Measurements can be used to introduce failures of the bonds in the orthotropic limits definition, as suggested in [5].

© 2023 IEEE. Personal use is permitted, but republication/redistribution requires IEEE permission. See https://www.ieee.org/publications/rights/index.html for more information.

This article has been accepted for publication in IEEE Transactions on Applied Superconductivity. This is the author's version which has not been fully edited and content may change prior to final publication. Citation information: DOI 10.1109/TASC.2023.3340126

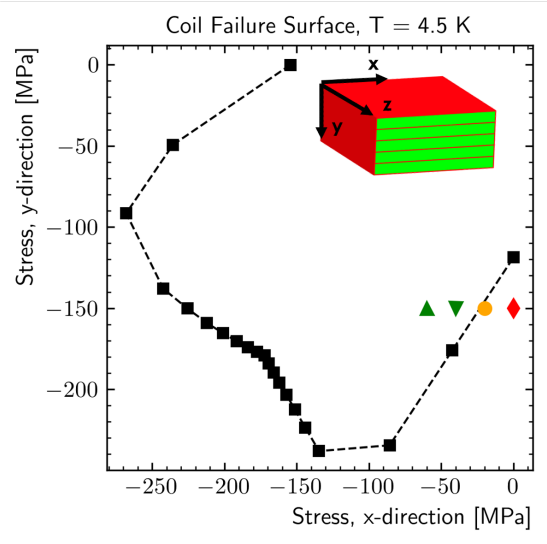


Fig. 3. Failure surface as computed on the coil model unconstrained longitudinally (z-direction), along with markers representing the experimental measurements performed on the bi-axial test set-up. N_c/N_s is the number of cracks per strand detected on on the samples tested at the loading conditions shown by the non-squared markers.

C. Multi-Axial Coil Strength

Testing the model with multiple load combinations, it is possible to define a failure surface at the coil level. For plane stress load configurations on the x-y plane, this produces the curve showed in Fig. 3 along with measurement results discussed in Section IV. The curve is very distant from the square that would represent the failure surface of an isotropic limit obtained from transversally loaded cable stacks (e.g. [6]); and also from the rectangle representing the 'orthotropic' failure criterion of Eq. 1. In particular, there is a significant strength increase under bi-axial loading conditions: according to this model, the filaments inside the strand could survive a transverse pressure of more than 200 MPa if a stress larger than 100 MPa is applied in the x-direction. This result seems consistent with measurements performed compressing strands in a groove, that showed no filaments failed after applying transversal pressures larger than 200 MPa [15]. In general, this model seems to confirm the idea that 'hydrostatic' loads are less dangerous, and that the deviatoric component of the stress is dominant in determining the crack formation and propagation within the coil composite. This last observation partially justifies the empirical limit on the Von Mises equivalent stress often used in the past.

III. Multi-Directional Loading Set-Up

A stack holder was designed to test the coil composite strength under bi-axial loading conditions. The design is shown in Fig. 4: two steel wings contain the sample laterally, and two screws are used to apply a load in the horizontal plane. The applied preload is controlled with bellville springs, that allow a rough measurement of the force, and to limit the variation of the force as a function of the bolt rotation. The configuration of the spring stack-up can be optimized to apply different loads. With the current configuration the set-up

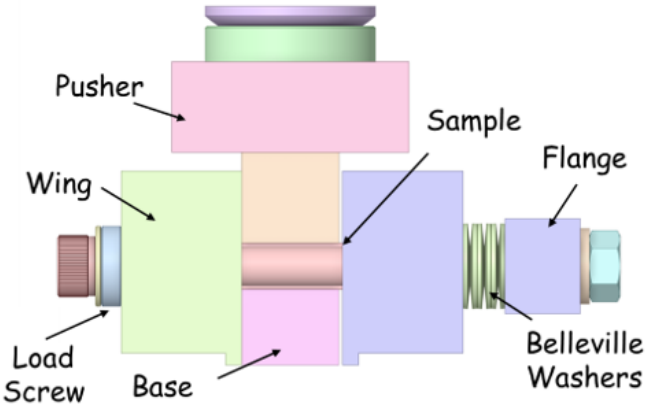


Fig. 4. Sample holder for bi-axial loading of cable stacks.



Fig. 5. Buckling failure of the first test specimen.

allows to apply a pressure ranging between 20 and 60 MPa on a stack of four MQXF cables.

Stacks of 250 mm long MQXF cables were reacted and impregnated using realistic reaction and impregnation fixtures, following the process described in [11]. A Teflon shim was introduced in the impregnation fixture, creating two 4-stack samples per fixture. The number of cables was chosen compromising between the need to have sufficient stack thickness, and to limit friction accumulation effects on the wing sides.

A diamond wire saw was used to cut the samples to an approximate length of 20 mm, discarding 10 mm from the head and tail of the stack. The samples were wrapped in 1 mm of polyamide to guarantee an uniform pressure distribution on the boundary. Additionally, HS (high) and HHS (ultra high) Fuji papers were applied on the bottom of the sample, and MS (medium) paper on the sides. The paper readings confirmed that the set-up applied a very uniform pressure on the sample sides. Additional Fuji paper was installed below the wings of the sample holder, to control that the load was correctly applied to the sample and not flowing through the wings because of frictional effects. Markings were not found on this additional paper after any of the experiments.

In a first assembly test, performed on one of the discarded stack ends, the test article buckled during the application of the horizontal prestress at around 15 MPa, as shown in Fig. 5. To avoid this effect, a vertical preload of 20 MPa was applied before torquing the screws on the real samples.

IV. Image Analysis Results

After loading, all samples were cold mounted in a clear epoxy, and polished initially with silicon carbide papers,

© 2023 IEEE. Personal use is permitted, but republication/redistribution requires IEEE permission. See https://www.ieee.org/publications/rights/index.html for more information.

This article has been accepted for publication in IEEE Transactions on Applied Superconductivity. This is the author's version which has not been fully edited and content may change prior to final publication. Citation information: DOI 10.1109/TASC.2023.3340126

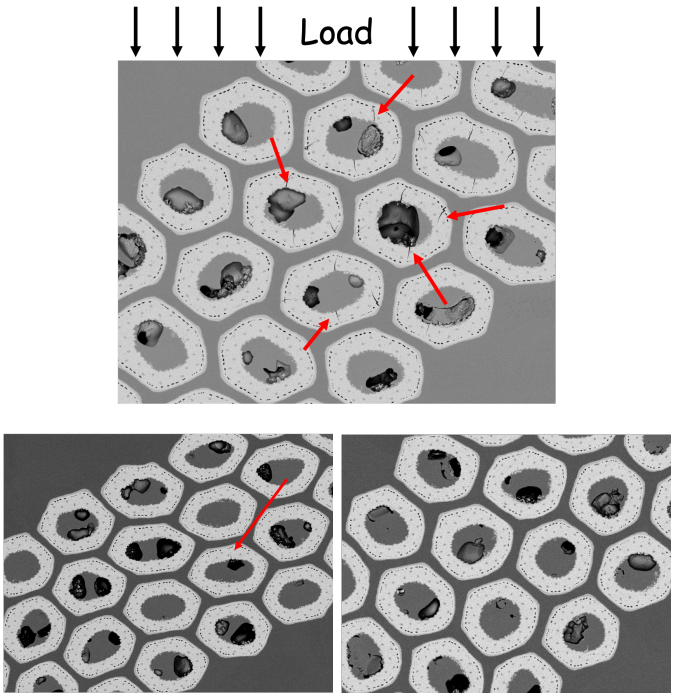


Fig. 6. Typical crack distributions in the samples after room-temperature loading at 150 MPa, with no lateral constraint (top), and with a 20 MPa (bottom left) and 40 MPa (bottom right) lateral load.

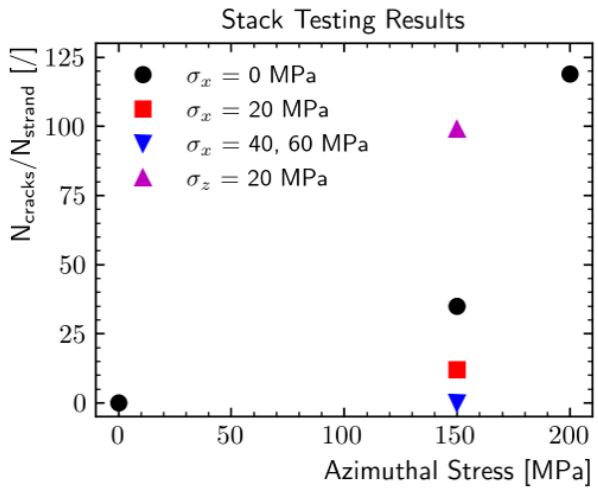


Fig. 7. Average number of cracks per strand detected from the image analysis, as a function of the azimuthal stress applied, and with different stresses in the radial (x) and longitudinal (z) direction. The radially loaded samples were left free along the longitudinal axis, and the longitudinally loaded ones along the radial axis.

removing 2–4 mm of material; then with diamond suspension solutions with a smallest particle size of 1 µm; and finally vibratory polished (0.05 µm particle size) overnight. A thin layer of Au-Pd was sputtered on the samples before imaging with a scanning electron microscope (Thermo Scientific™ Scios™ 2 DualBeam™). All images were acquired at a magnification of 350x using an in-lens detector (T2) with dominant backscattered electron signal to maximize phase contrast and to ease crack identification. High resolution images (around 27 megapixels) were saved to locate all cracks in a strand from a single image.

An initial run was performed applying a load in the azimuthal direction to the unconfined sample at room temperature. The load levels tested were: 100, 125, 150, 175 and 200 MPa. The cracks started on the 125 MPa sample: this seems consistent with the numerical model prediction that crack would propagate at 115 MPa with this load configuration (see Section II).

Afterwards, new samples were subject to bi-axial loading conditions, also at room temperature. As the horizontal stress was increased, the cracks gradually disappeared, as shown for a representative filamentary region of three samples in Fig. 6. The number of cracks found on the samples are reported in Fig. 7. The crack number decreased significantly when an horizontal stress was applied: from 100 cracks per strand with a 0 MPa prestress, to 15 at 20 MPa, to 0 at 40 MPa. The sample with a prestress of 60 MPa also had no visible cracks. Reporting these sample points with colored markers on the failure surface of Fig. 3 highlights a remarkable agreement with the numerical model in this particular load region: cracks diminish when approaching the failure surface, and disappear when entering the no-failure region.

These measurements seem to confirm the expected strong interaction between azimuthal (y-direction in Fig. 3) and radial (x) stress in defining the strength limits of the conductor. One data point was also obtained applying a longitudinal (z) prestress on the sample, this time free in the radial direction. This measurement shows an increase of the cracks per strand with respect to the uni-axially loaded sample. Additional testing is needed to confirm this result on more samples. Furthermore, it is unclear if the longitudinal load might have beneficial effects in preventing the propagation of the cracks in the longitudinal direction.

V. Conclusion

Defining the coil strength as the stress level at which radial cracks propagate in the filaments, numerical models and measurements were used to define the limits under uni-axial and bi-axial loading conditions. Measurements, performed on cable stacks, showed cracks on-set between 100 and 125 MPa under the same loading conditions. The model, built using a multi-scale methodology, predicted a stress limit of 115 MPa for stacks under transverse loads.

The numerical methodology was also used to define a failure surface for the coil composite. The surface shape suggests that limits for ‘hydro-static’ loading conditions might be significantly higher than the ones typical of uni-axial loads. Measurements showed that, as predicted by the numerical model, cracks disappeared when the horizontal prestress was increased. The load combination necessary to prevent crack formation also seems in good agreement with the numerical results.

While further data points are required to characterize the failure surfaces at room temperature and at cold, these early results could already help in practical magnet design tasks, for example in the definition of critical areas and optimal preload conditions.

© 2023 IEEE. Personal use is permitted, but republication/redistribution requires IEEE permission. See https://www.ieee.org/publications/rights/index.html for more information.

This article has been accepted for publication in IEEE Transactions on Applied Superconductivity. This is the author's version which has not been fully edited and content may change prior to final publication. Citation information: DOI 10.1109/TASC.2023.3340126

REFERENCES

[1] B. Bordini, P. Alknes, L. Bottura, L. Rossi, and D. Valentinis, "An exponential scaling law for the strain dependence of the Nb_3Sn critical current density," *Superconductor Science and Technology*, vol. 26, no. 7, p. 075 014, 2013.

[2] G. Vallone, B. Bordini, and P. Ferracin, "Computation of the reversible critical current degradation in Nb_3Sn Rutherford cables for particle accelerator magnets," *IEEE Transactions on Applied Superconductivity*, vol. 28, no. 4, 2018.

[3] G. Vallone *et al.*, "A methodology to compute the critical current limit in Nb_3Sn magnets," *Superconductor Science and Technology*, vol. 34, no. 2, 2020.

[4] G. Vallone *et al.*, "Computation of the strain induced critical current reduction in the 16 T Nb_3Sn test facility dipole," *IEEE Transactions on Applied Superconductivity*, vol. 33, no. 5, pp. 1–5, 2023.

[5] G. Vallone, E. Anderssen, B. Bordini, and P. Ferracin, "A review of the mechanical properties of materials used in Nb_3Sn magnets for particle accelerators," *IEEE Transactions on Applied Superconductivity*, vol. 33, no. 5, pp. 1–6, 2023.

[6] P. Ebermann *et al.*, "Irreversible degradation of Nb_3Sn Rutherford cables due to transverse compressive stress at room temperature," *Superconductor Science and Technology*, vol. 31, no. 6, p. 065 009, 2018.

[7] H. Felice *et al.*, "Performance of a Nb_3Sn quadrupole under high stress," *IEEE Transactions on Applied Superconductivity*, vol. 21, no. 3, pp. 1849–1853, 2011.

[8] S. W. Tsai, "Strength theories of filamentary structure," *Fundamental aspects of fiber reinforced plastic composites*, 1968.

[9] S. W. Tsai and E. M. Wu, "A general theory of strength for anisotropic materials," *Journal of Composite Materials*, vol. 5, no. 1, pp. 58–80, 1971.

[10] S. Pinho, R. Darvizeh, P. Robinson, C. Schuecker, and P. Camanho, "Material and structural response of polymer-matrix fibre-reinforced composites," *Journal of Composite Materials*, vol. 46, no. 19-20, pp. 2313–2341, 2012.

[11] C. Fichera *et al.*, "New methodology to derive the mechanical behavior of epoxy-impregnated Nb_3Sn cables," *Ieee Transactions on Applied Superconductivity*, vol. 29, no. 7, 2019.

[12] S. Krave, T. Shen, and A. Haight, "Exploring new resin systems for Nb_3Sn accelerator magnets," *IEEE Transactions on Applied Superconductivity*, vol. 31, no. 5, 2021.

[13] G. Vallone and P. Ferracin, "Modeling coil-pole debonding in nb3sn superconducting magnets for particle accelerators," *IEEE Transactions on Applied Superconductivity*, 2017.

[14] G. Vallone *et al.*, "Modeling training in Nb_3Sn superconducting magnets," *IEEE Transactions on Applied Superconductivity*, no. 5, pp. 1–5, under review.

[15] T. Bagni, D. Mauro, M. Majkut, A. Rack, and C. Senatore, "Formation and propagation of cracks in RRP Nb_3Sn wires studied by deep learning applied to x-ray tomography," *Superconductor Science and Technology*, vol. 35, no. 10, p. 104 003, 2022.

[16] A. Moros *et al.*, "A metallurgical inspection method to assess the damage in performance-limiting Nb_3Sn accelerator magnet coils," *IEEE Transactions on Applied Superconductivity*, vol. 33, no. 5, pp. 1–8, 2023.

[17] P. Ferracin *et al.*, "The HL-LHC low-β quadrupole magnet MQXF: From short models to long prototypes," *IEEE Transactions on Applied Superconductivity*, vol. 29, no. 5, pp. 1–9, 2019.

[18] N. Cheggour, T. C. Stauffer, W. Starch, L. F. Goodrich, and J. D. Splett, "Implications of the strain irreversibility cliff on the fabrication of particle-accelerator magnets made of restacked-rod-process Nb_3Sn wires," *Scientific Reports*, vol. 9, no. 1, p. 5466, 2019.

© 2023 IEEE. Personal use is permitted, but republication/redistribution requires IEEE permission. See https://www.ieee.org/publications/rights/index.html for more information.